Radiation and Electromagnetic Induction Data Fusion for Detection of Buried Radioactive Metal Waste – 12282

Zhiling Long[1], Wei Wei[1], Anish Turlapaty[1], Qian Du[1], Nicolas H. Younan[1], and Charles Waggoner[2]

[1]Department of Electrical and Computer Engineering
[2]Institute for Clean Energy Technology
Mississippi State University, MS 39762, USA

ABSTRACT

At the United States Army's test sites, fired penetrators made of Depleted Uranium (DU) have been buried under ground and become hazardous waste. Previously, we developed techniques for detecting buried radioactive targets. We also developed approaches for locating buried paramagnetic metal objects by utilizing the electromagnetic induction (EMI) sensor data. In this paper, we apply data fusion techniques to combine results from both the radiation detection and the EMI detection, so that we can further distinguish among DU penetrators, DU oxide, and non-DU metal debris. We develop a two-step fusion approach for the task, and test it with survey data collected on simulation targets.

INTRODUCTION

DU is both toxic and radioactive. Due to its high density and pyrophoricity, the material has been made into military weapons such as armor piercing penetrator rounds. At the United States Army's test sites, there are fired DU penetrators buried under ground surface over the years. They become hazardous waste and need to be removed. Therefore, it is very important to develop technologies for locating these buried DU penetrators in the field. At the same time, it is also of interest to know the state of oxidation of the buried penetrators. DU oxides have higher mobility than DU penetrators. Thus, they are more easily to pollute the environment.

For the past several years, we have been working on development of suitable techniques to address this challenging task. We developed approaches based on signal processing techniques such as matched filtering [1, 2], for successful detection of buried radioactive targets. We also developed methods for locating buried paramagnetic metals by utilizing the EMI sensor data [3]. With the radiation detection, we can locate radiation sources, but cannot easily distinguish between DU and oxides. Although EMI detection can identify DU among other metals, it cannot detect if any oxides are in existence. We believe that combination of results from these two types of detection will help further distinguish among DU, oxides, and non-DU metal debris.

To achieve this objective, we can utilize data fusion techniques that have been widely adopted in remote sensing and wireless sensor networks. Data fusion seeks to improve quality of

information obtained from multiple sources by combining them in various manners [4]. For object detection or classification applications, typical data fusion techniques fall into two categories. One is feature level fusion, which integrates features extracted from raw data from different sources. The other is decision level fusion, which fuses detection or classification decisions from each source. In this work, we adopt typical decision level fusion techniques, such as majority voting (MV) [5], to integrate results from both radiation and EMI detections. We develop a two-step approach and test it with data acquired on simulation targets. Our fused results can successfully reveal locations for detected DU, oxide, and non-DU metals.

APPROACH

Radiation Detection

We have had success in conducting radiation detection by using gamma spectroscopy collected from sodium iodide (NaI) scintillation detectors [1, 2]. In this work, we utilize the conventional RX algorithm to process the spectral data for the detection. In the RX algorithm [6], a nonstationary local mean is subtracted from each spectral pixel within a fixed window. The local mean is obtained by sliding a double concentric window, which consists of a small inner window centered within a larger outer window over each pixel in an image. The mean is then calculated from the spectral pixels falling between the inner and the outer windows. The size of the inner window is usually assumed to be the size of the target of interest. The residual signal after mean subtraction is assumed to approximate a zero-mean Gaussian random process. Let each input signal vector be denoted by $\mathbf{x} = [x_1, x_2, ..., x_n]^T$, then a two-hypothesis test is formulated as

$$H_0 : \mathbf{x} = \mathbf{n},$$

(Eq. 1)

$$H_1 : \mathbf{x} = a \cdot \mathbf{s} + \mathbf{n},$$

(Eq. 2)

where $\mathbf{n}$ is a noise vector representing the background noise process, $\mathbf{s}$ is a feature signal representing the anomaly signal, and a is a constant, which is greater than 0 under hypothesis H_1 and equals to 0 under H_0.

The target signature and background covariance are assumed to be unknown. This model assumes that the data come from two normal probability density functions with the same covariance matrix but different means [7]. Under H_0, the data (background clutter) are modeled as $N(\mathbf{0}, \mathbf{C}_b)$, and under H_1 the data are modeled as $N(\mathbf{s}, \mathbf{C}_b)$. It should be noticed that an important assumption in the RX-algorithm is that the background and target have the same covariance matrix. Generally, this is not a valid model if a particular target structure is to be detected. A more appropriate model would have two different covariance structures — one for the anomaly (which could be target or background clutter) and the other for the background. However, the covariance structure for the anomaly cannot be estimated in reality, since the

statistical structure of the anomaly signals cannot be defined. Therefore, the same covariance structure for the anomaly and the background is adopted.

The basic RX algorithm can be written as below:

$$w_{RX} = (\mathbf{x} - \boldsymbol{\mu})^T \mathbf{R}^{-1} (\mathbf{x} - \boldsymbol{\mu})$$ (Eq. 3)

where $\mathbf{R}$ is the background covariance matrix estimated from the surrounding background data, and $\boldsymbol{\mu}$ is the estimated background clutter sample mean [8]. A threshold η is to be assigned such that detection can be achieved on the RX output.

EMI Detection

According to Maxwell's laws a permeable object is induced with eddy currents by a time-variant H field. The object later generates its own secondary H field. For compact objects with well defined shapes such as spheres and cylinders, this H-field can be derived using analytical methods as presented in [9]. EMI spectroscopy measures this secondary H-field as a function of frequency and analyzes it to determine the object's EM properties. It has been widely used in commercial applications for detection of unexploded ordinances (UXO) and landmines [10].

In this work, we utilize Geophex's GEM-3 sensor for EMI detection [11]. The H-field measured by the GEM-3 sensor can be presented as

$$H = f(geometry)(I + jQ)$$ (Eq. 4)

Here, the $f(geometry)$ factor depends on the target/sensor geometry, I represents the inphase component of the EMI response, and Q is the quadrature component. Both I and Q are related to the material properties of the target [9, 12].

Let Q_a be the quadrature component of a background adjusted H-field measured using the GEM-3 sensor, and our EMI detection algorithm consists of three steps as follows [3].

a) Concavity Test for Metal Signatures

For the frequencies involved in the measurements of this study, the quadrature component of most metals usually has only one peak. Thus it may have a concave structure. The concavity of a signal Q_a can be easily tested by using its second derivate. If $Q_a^{''} < 0$, then the signal has a concave shape.

b) Peak Magnitude Test for Separation from Background

The Q component of the EMI response of a compact permeable object should have a peak that is usually greater than the peak of the background noise Q_{BGPeak}. Therefore, by this peak

magnitude test we can separate a permeable object from the background. Normally Q_{BGPeak} has to be determined from the data empirically.

c) Matching with a Library of Known Signatures to Identify the Targets

From the above two steps, we can know if the signal Q_a represents a permeable metal object. To further determine the nature of the metal object, the signal is compared with a library of quadrature components of known metals including DU. By evaluating the separation between the peak frequency of the object (pf_{target}) and those of the signatures in the library (pf_{metal}) using the metric

$$D_{t\,\arg et} = \left(pf_{t\,\arg et} - pf_{metal}\right)^2 ,$$ (Eq. 5)

we identify the object of interest as the metal whose signature provides the best match.

Radiation and EMI Data Fusion

To fuse the radiation detection results with the EMI detection results, first of all, we need to cope with the situation of mismatch between the survey lines. Currently the radiation survey and the EMI survey are performed separately. If at a certain location we have only a result from one type of detection, then fusion cannot be conducted for that location. As defined by the resolution of the coordinates obtained from the surveying systems, the survey grid size is 1cm by 1cm. When we perform the fusion, we re-grid the survey area by setting a grid size reasonable larger than this survey grid size. This way, mismatch survey paths may fall into the same grids if they are located close enough.

As illustrated in Figure 1, our fusion approach consists of two steps. In the first step, we fuse radiation detection results and EMI detection results separately. After re-gridding the survey area by increasing the grid size, often times there will be several survey results falling into a same grid. We examine all radiation detection results inside a certain grid, and determine if we should assign "radiation" or "non-radiation" to the grid by majority voting (MV) [5]. Similarly, we examine all EMI detection results inside the grid and vote for that grid to be "DU," "non-DU metal," or "non-metal."

In the second step of the fusion, we combine the radiation detection decision from the first step with the EMI detection decision. This fusion follows the rules below:

a) If EMI decision is "DU" and radiation decision is "radiation", then final decision is "DU";
b) If EMI decision is "DU" and radiation decision is "non-radiation", then final decision is "DU";
c) If EMI decision is "non-DU metal" and radiation decision is "radiation", then final decision is "oxide";

4

d) If EMI decision is "non-DU metal" and radiation decision is "non-radiation", then final decision is "non-DU metal";

e) If EMI decision is "non-metal" and radiation decision is "radiation", then final decision is "oxide";

f) If EMI decision is "non-metal" and radiation decision is "non-radiation", then final decision is "background".

We note that for rule b) above, the EMI decision is actually in contradiction to the radiation decision. In this case, we choose the decision to be "DU" to avoid missing any possible DU targets. Similarly, in rule c), we choose to assign "oxide" instead of "non-DU metal" to the grid, so that we will not miss any possible radiation sources.
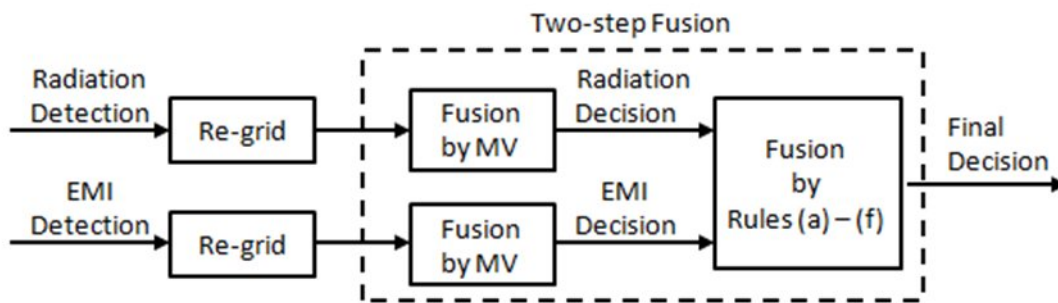
Figure 1. Illustration of the two-step fusion approach.

RESULTS

Datasets

To test the performance of our radiation and EMI data fusion approach, we perform preliminary experiments involving simulation targets. We place a group of targets in a parking lot and survey the area with both radiation and EMI detectors. As illustrated in Figure 2, the targets include DU (big and small), DU oxides, and metallic objects such as aluminum, brass, copper, and steel. The radiation survey includes 16 parallel paths and 7477 measurements, while the EMI survey is also along 16 parallel paths but consists of a total of 4205 measurements.

Radiation Detection

We applied the RX algorithm to the radiation survey data. The threshold η used for the detection was empirically set to be 280. The detection results are shown in Figure 3. From the figure, we can see that almost all DU targets and oxides were detected, except for two small DU targets that were placed away from the survey path. There are also some false alarms, but they are basically located around true targets, especially the two big DU targets. The non-DU metals are not radioactive, thus undetectable in this survey.
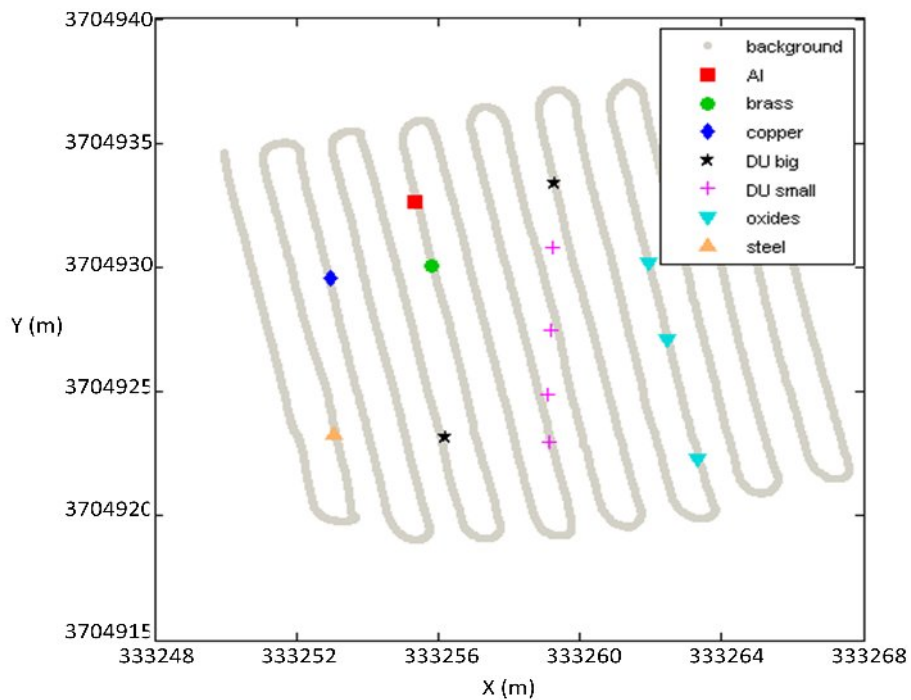
Figure 2. Distribution of simulation targets along the EMI survey path.
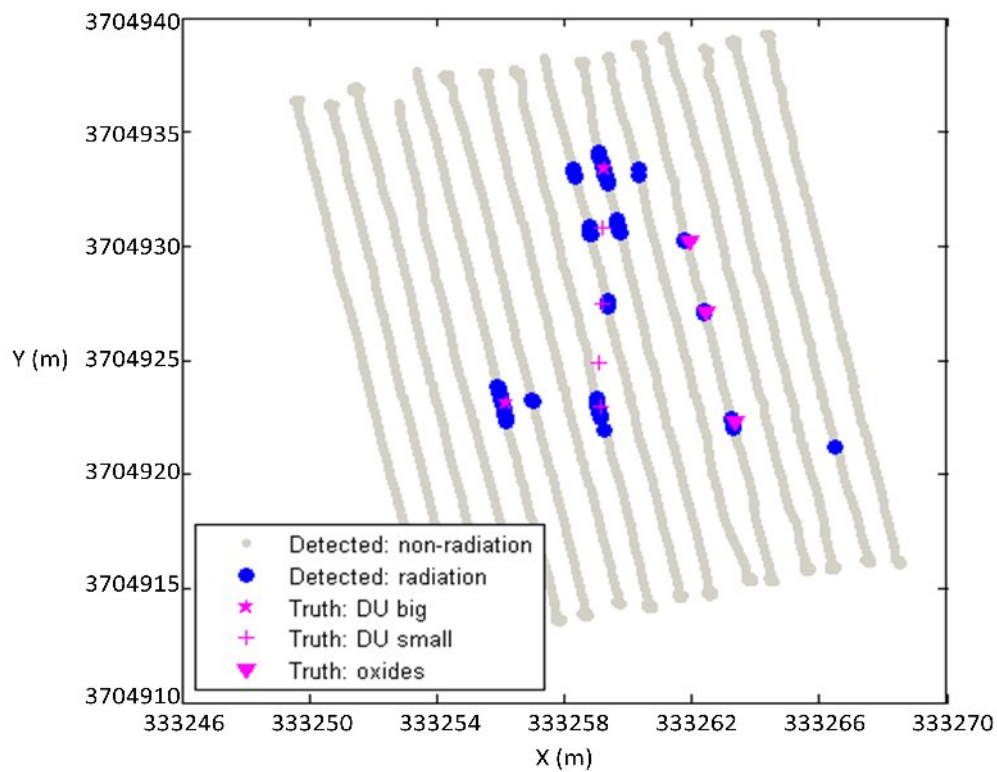
Figure 3. Results of radiation detection with ground truth information.

EMI Detection

We applied our three-step analysis approach to the EMI spectroscopy survey data. The detection results are presented in Figure 4. As we can see, most of the targets including DU, copper, brass and steel were all detected and identified correctly. Several small DU targets that are located away from the survey line were not detected. Since oxides do not have any magnetic properties, they were not detected by the EMI survey and were missing from the detection results.
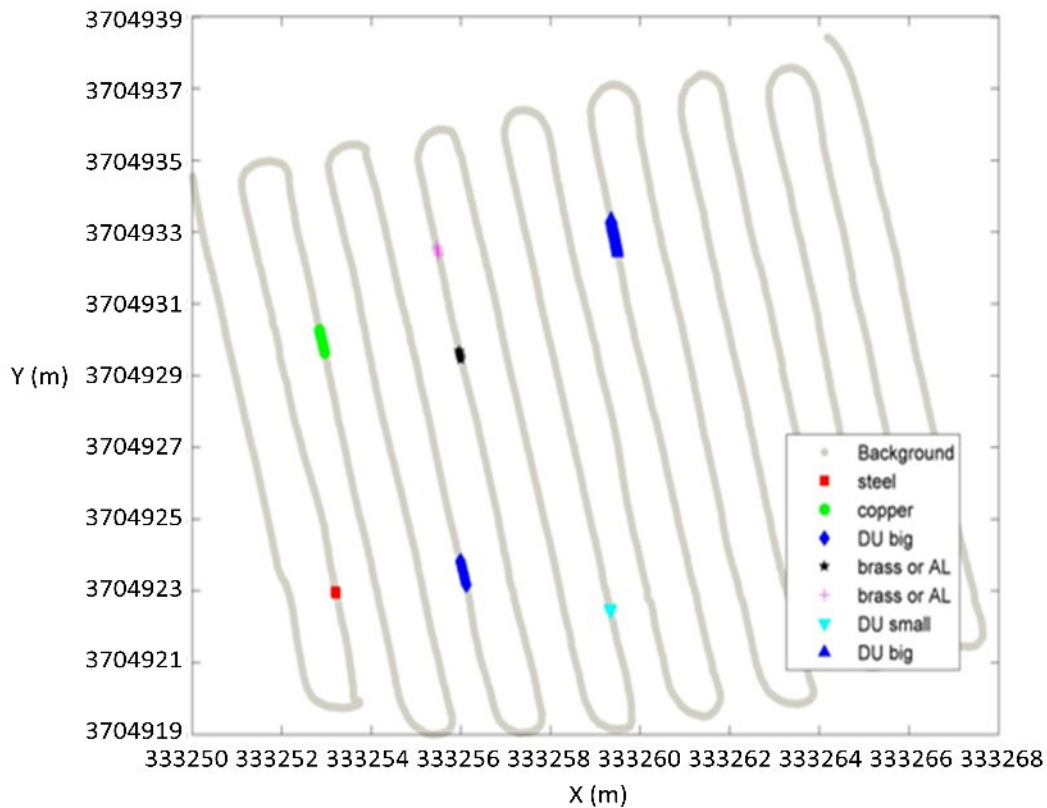
Figure 4. Results of EMI detection. For ground truth information, refer to Figure 2 above.

Radiation and EMI Data Fusion

For the re-gridding, we set the grid size to be 25cm by 25cm (about 10" by 10"). By applying our two-step fusion approach to the radiation detection and EMI detection results, we obtain the fused map (Figure 5) showing locations of DU, oxides, and non-DU metals. We observe that the majority of the simulation targets were located and identified correctly in the map. For DU, three out of the six were detected. The three missing ones are small and off the survey path. For oxides, two out of the three were detected. The only missing one has been identified as a radiation source in the radiation detection, but was voted out in the fusion process. The non-DU metals were also detected successfully, with only one of them missing in the fused map. Similarly, that one was detected in the EMI survey, but was not kept in the fusion process. There

are some false alarms in the fusion results, especially for the oxides. However, these false detections of oxides are all around DU targets, which is reasonable. They are actually carried over from the radiation detection results. An improved radiation detection algorithm will help reduce these false alarms in the fusion.
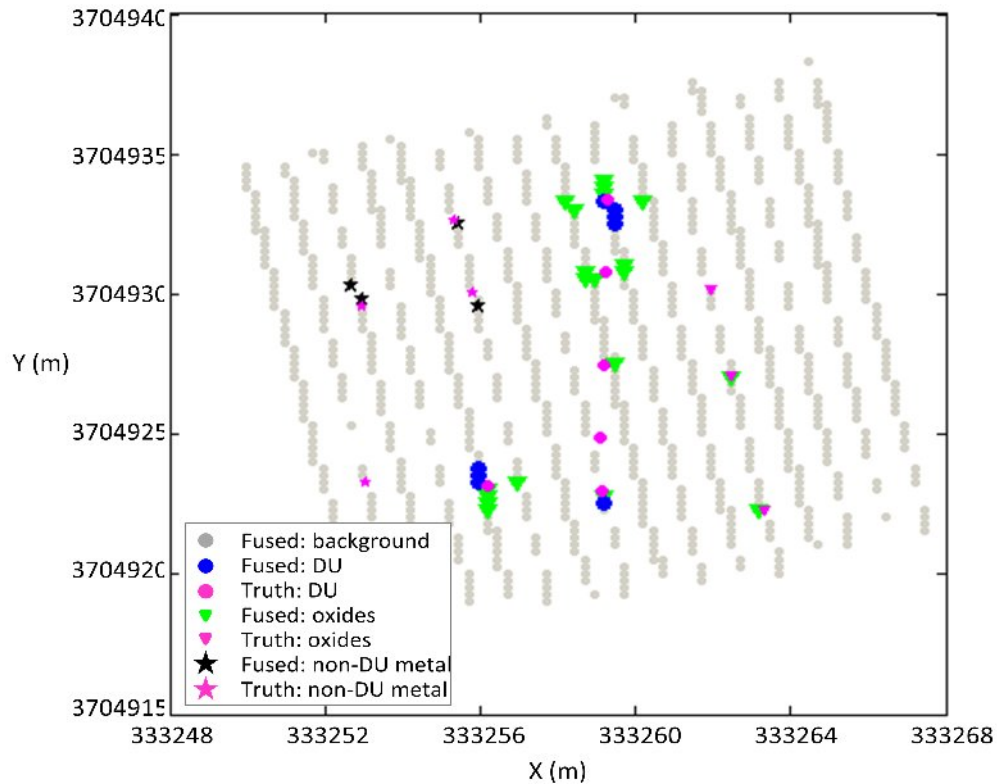
Figure 5. Results of radiation and EMI data fusion with ground truth information. The ground truth markers are all colored in magenta. They are of the same shape as markers for the corresponding fusion results.

CONCLUSIONS

In this work, we explored radiation and EMI data fusion for detecting DU, oxides, and non-DU metals. We developed a two-step fusion approach based on majority voting and a set of decision rules. With this approach, we fuse results from radiation detection based on the RX algorithm and EMI detection based on a 3-step analysis. Our fusion approach has been tested successfully with data collected on simulation targets. In the future, we will need to further verify the effectiveness of this fusion approach with field data.

REFERENCES

1. Q. Du, N. H. Younan, C. Waggoner, and D. Rogers, "Effective Detection of Buried Radioactive Waste," Proceedings of Waste Management Conference (2009).

2. Q. Du, W. Wei, Z. Huang, N. H. Younan, C. Waggoner, and D. Rogers, "Enhanced Effective Detection of Buried Radioactive Waste," Proceedings of Waste Management Conference (2010).

3. A. C. Turlapaty, Q. Du, and N. H. Younan, "Detection and Classification of Buried Radioactive-metal Objects Using Wideband EMI Data," Proceedings of IEEE International Geoscience & Remote Sensing Symposium (2011).

4. E. Nakamura, A. Loureiro, and A. Frery, "Information Fusion for Wireless Sensor Networks: Methods, Models, and Classifications," ACM Computing Surveys, vol. 39, no. 3, Article 9, Aug. 2007.

5. H. Yang, Q. Du, and B. Ma, "Decision Fusion on Supervised and Unsupervised Classifiers for Hyperspectral Imagery," IEEE Geoscience and Remote Sensing Letters, vol. 7, no. 4, pp. 875-879, Oct. 2010.

6. H. Kwon and N. M. Nasrabadi, "Kernel RX-algorithm: a Nonlinear Anomaly Detector for Hyperspectral Imagery," IEEE Transactions on Geoscience and Remote Sensing, vol. 43, no. 2, pp. 388-397, 2005.

7. C. I. Chang and S.-S. Chiang, "Anomaly Detection and Classification for Hyperspectral Imagery," IEEE Transactions on Geoscience and Remote Sensing, vol. 40, no. 2, pp. 1314-1325, 2002.

8. W. H. Farrand and J.C. Harsanyi, "Mapping the Distribution of Mine Tailing in the Coeur d'Alene river Valley, Idaho through the Use of Constrained Energy Minimization Technique," Remote Sensing of Environment, vol. 59, no. 1, pp. 64-76, 1997.

9. F. S. Grant, and G. F. West, "Theory of Electromagnetic Induction," in: Interpretation Theory in Applied Geophysics, pp. 486-547, McGraw-Hill Book Company, New York, 1965.

10. I. J. Won, D. A. Keiswetter, and T. H. Bell, "Electromagnetic Induction Spectroscopy for Clearing Landmines," IEEE Transactions on Geoscience Remote Sensing, vol. 39, no. 4, pp. 703–709, 2001.

11. I. J. Won, D. Keiswetter, D. Hanson, E. Novikova, and T. Hall, "GEM-3: a Monostatic Broadband Electromagnetic Induction Sensor," Journal of Environmental Engineering & Geophysics, vol. 2, no. 1, pp. 53–64, 1997.

12. J. T. Miller, T. H. Bell, J. Soukup, and D. Keiwetter, "Simple Phenomenological Models for Wideband Frequency-domain Electromagnetic Induction," IEEE Transactions on Geoscience and Remote Sensing, vol. 39, no. 6, pp. 1294-1298, 2001.

ACKNOWLEDGMENT